Bio-Based Sandwich Beams made of Paper Honeycomb Cores and Flax FRP Facings: Flexural and Shear Characteristics

Yuchen Fu and Pedram Sadeghian[1]

Department of Civil and Resource Engineering, Dalhousie University, Halifax, NS, Canada

ABSTRACT:

Sandwich composite panels have been used in construction as building envelopes and cladding systems. The sandwich composite used today are mainly made of conventional synthetic foam cores and synthetic fiber-reinforced polymer (FRP) facings, typically made of glass or carbon fibers and synthetic polymers. With increasing environmental consciousness, it is important to develop sustainable building materials to replace conventional building materials with more sustainable materials such as bio-based fibers and polymers. There is lack of studies on sandwich composites made of bio-based materials for both core and facings. In this study, 18 sandwich beam specimens (1200 mm long and 100 mm wide) made of flax FRP facings and 75 mm thick paper honeycomb core were fabricated and tested under three-point bending. The parameters of the tests were facing thickness (1, 2 and 3 layers of flax FRP) and core types (hollow and foam-filled). It was found that the paper honeycomb has comparable performance with lighter weight to other synthetic counterparts and foam-filling was effective in improving the performance of the core and sandwich beams. In addition, as the nonlinear behavior of the specimens was evident, a new analytical model was developed based on the material

---

[1] *Corresponding Author: Pedram Sadeghian, Associate Professor and Canada Research Chair in Sustainable Infrastructure, Department of Civil and Resource Engineering, Dalhousie University, Halifax, NS, Canada. Email: Pedram.sadeghian@dal.ca*

nonlinearity of both facings and core materials to predict the test data and perform a parametric study. Overall, the bio-based sandwich system showed substantial potential to be used for building applications with much less environmental footprints in comparison with other synthetic counterparts.

1. INTRODUCTION

With the development of industry and the growth of populations, the average of 13,000 buildings will be built daily from now to 2050 [1]. About 40% of global raw material is expended by the building industry and about 50% of carbon dioxide released into the atmosphere comes from the construction sector [2]. With the growing understanding of the impact on the environment caused by human activity, we need to find ways to make building construction more sustainable. In recent years, our desire to find a renewable material to replace synthetic materials, and the number publications of bio-based materials and applications have been sharply increased [3]. Synthetic fibers such as glass fiber [4] and recycled plastic-based fibers [5][6] have been used in the past, however the use of natural fibers have been limited. Research on polymers has also been transformative and new generations of adhesive materials with increased toughness [7] and bio content [8] have been developed. Over 100 years ago, natural fibers composites were used for airplane seats and fuel-tanks, tubes, and pipes for electronic purposes [9]. There are mainly five types of natural fibers: bast fibers, leaf fibers, core fibers, grass, and reed fibers. Flax fiber is a bast fiber, and it is the most widely used in

the composites field [10]. Chemical composition (by weight) of flax fibers are 71% cellulose, 18.6-20.6% hemicellulose, 2.2% lignin, and 1.5% waxes. The tensile strength and Young's modulus were reported as 345-1035 MPa and 27.6 GPa, respectively [10]. Comparing to conventional materials (E-glass and carbon), the natural materials are more eco-friendly as they are more renewable, recyclable, reusable, and biodegradable. Because of its lightweight, lower energy is required during the transportation and installation [11][12]. Moreover, it has potential to be used together with bio-based polymers to make bio-based Fiber reinforced polymer (FRP) composites [13][14][15] for a variety of application including sandwich composite panels for building envelopes.

A sandwich composite consists of a thick core and two thin facing materials, and it is a very effective system with high stiffness/strength and minimum weight. The core is normally lightweight and separates the strong facing materials apart to provide higher moment of inertia under flexure, and it also provides shear resistance and insulation (heat and sound). The two facings are very stiff and strong to resist tension and compression forces resulting from a bending moment [16][17]. Nowadays, sandwich composites made by FRP facings and core have been practices for couple decades. The conventional fiber used for FRPs are synthetic, such as carbon and glass fiber [18][19]. The most popular core materials are synthetic foams and honeycombs. Compared with an FRP made by synthetic fibers, an FRP made by natural fibers has lower modulus and strength. However, because of the relatively lower strength of core materials, the failure of sandwich structure is usually governed by the core, which means the FRP facings rarely reach their ultimate strength. Therefore, the high strength of synthetic fibers is not fully utilized in most cases [20]. Therefore, a lower strength, but more

environmentally friendly, natural fibers can be used to replace conventional synthetic fibers. In this study, flax was used for manufacturing the FRP facing. Flax is readily available and has relatively higher strength and stiffness than other natural fibers [21]. On the other hand, a hhoneycomb structure is a gift from nature. The hexagonal cell structure contains large space to minimize weight and high performance [22][23]. Most of the research and applications have been focused on honeycombs made of synthetic materials such as aluminum, plastics, and aramid composites; however, honeycombs made of paper-based materials have shown potential as an alternative. The sustainability of sandwich composites can be improved by using paper-based honeycombs as approximately 85% of corrugated cardboard in Canada is recycled and new cardboard is produced with nearly 100% recycled materials [24].

Numerous research has been conducted on sandwich composites made of synthetic FRP facings and core materials [25][26][27][28]. Using bio-based FRP facings and synthetic foam core has also gained significant attention [20][29][30][31]. However, there are very limited studies on the sandwich composites made of fully bio-based material for both facings and core components. Recently, small-scale bio-based sandwich beams with flax FRP facings and corrugated cardboard core were tested under four-point bending by McCracken and Sadeghian [24]. Then, Betts et al. [32] tested similar but larger scale sandwich beams under static and impact bending load. Balsa wood has also been used as core material [33]. Recently, flax FRP facings and paper honeycomb core has been used for small-scale specimens under bending [34], but the thickness of paper honeycomb ranged from 6 to 25 mm, which is not applicable for building envelope where much higher thickness is needed for both structural and insulation requirements. The research gap of the performance of large-scale sandwich beams made of flax

FRP facings and thick paper honeycomb core is evident. The testing of large-scale specimens will also eliminate any potential influence caused by size effects. The significance of this study is to fill the research gap via testing the structural performance of bio-based sandwich beams made of flax FRP facings and 75 mm thick paper honeycomb core (hollow and foam-filled), which has not been conducted in the past. Also, a new analytical model is developed to consider the material nonlinearity of both facings and core components towards a parametric study.

2. EXPERIMENTAL PROGRAM

2.1. Test Matrix

A total of 18 sandwich beams (1200 mm long and 100 mm wide) made of flax FRP facings and 75 mm thick paper honeycomb core was fabricated as shown in Table 1. The main parameters were the facing thickness and the type of paper honeycomb core (hollow and foam-filled). Three facing thicknesses were studied, namely: one, two, and three layers of flax FRP on each side of the sandwich beams. The thickness of each layer was measured to be approximately 1.5 mm. Two types of paper honeycomb core were examined: hollow and manually filled with foam. As shown in Table 1, a total of six cases were considered, and three identical specimens per case were fabricated and tested. A specimen identification system with format of XFL-Y is used to identify each specimen. X is the number of flax FRP layers in each face, and FL represents "Flax Layers". Y indicates the core type, where F is foam-filled, and H is hollow. The length and width of the specimens and the thickness of the core material was selected to be similar to the previous study by Betts et al. [20]. The type of skin and epoxy were also selected to be compatible with the study. The main parameter considered in the current is the use of paper honeycomb core rather than a synthetic foam core.

2.2. Material Properties

The flax FRP was fabricated using a bidirectional flax fabric (Biotex Flax, Composites Evolution, Chesterfield, UK) with a density of 410 g/m^2 and a bio-based epoxy resin with a bio-content of 21% after mixing (SuperSap, Entropy Resins, Hayward, CA, US). The flax FRPs were previously tested by Betts et al. [20] according to ASTM D3039 [35]. Although, the bio content of the bio-based epoxy resin used by Betts et al. [20] was 30% and that of the bio-based used in the current study is 21%, the mechanical properties of the resins are the same per the manufacturer. The tensile modulus, strength, and ultimate strain of the flax FRP were obtained 7.51 GPa, 45.4 MPa and 0.0083 mm/mm, respectively.

A paper honeycomb (Joy Business CO, LTD, Jiashan, Zhejiang, China) with the thickness of 75 mm was used as the core material. The paper honeycomb was shipped by the manufacturer in unstretched form after stretching, the honeycomb was filled with a spray foam (Quad Max Foam, LePage, Mississauga, ON, Canada) for half of the test specimens as shown in Table 1. The density of fully stretched hollow and foam-filled paper honeycomb core were measured to be 19 and 44 kg/m^3, respectively. Three hollow and three foam-filled honeycomb cores were tested in shear per ASTM C273 [36] and the stress-strain curves are shown in Figure 1. For the hollow honeycomb core, the shear modulus, ultimate shear strength, and corresponding strain were tested to be 10.24 MPa, 150 KPa, and 0.037 mm/mm respectively. For the foam-filed honeycomb core, the shear modulus, ultimate shear strength, and corresponding strain were tested to be 12.73 MPa, 240 KPa, and 0.039 mm/mm, respectively.

2.3. Specimen Fabrication

The paper honeycomb cores were shipped in unstretched form, as shown in Figure 2(a). The

stretch direction is the weak direction of the honeycomb core. Therefore, the weak direction of the core was selected to be the testing direction, as shown in Figure 2(b). For the foam-filled honeycomb cores, the spray foam was filled into the cells of the hollow paper honeycomb core by a foam dispensing gun as shown in Figure 2(c). After 6 hours of curing in room temperature, a Surform Plane was used to remove extra foam on both sides of the honeycomb, as shown in Figure 2(d). The final product is shown in Figure 2(e).

All the sandwich panels followed the same fabrication procedure. Firstly, the flax was cut to the proper dimensions by scissors. Parchment paper was taped on a clean table surface to make sure the facings of final products are flat and easy to separate from table after resin is fully cured. Once a layer of parchment paper was applied on a flat surface, the bio-based resin was mixed with hardener at a ratio of 100:43 by weight and applied to the parchment paper. The brushes were used to evenly spread the mixed resin on the parchment paper. Then, the first layer of flax fabric was applied to the wetted parchment paper with the warp direction of the fabric parallel to the longitudinal direction of the specimen. Then, another layer of bio-based epoxy resin was applied to the flax fabric to make the fabric fully saturated. Based on the desired flax FRP layers, more flax fabric layers were applied in the same process. After the desired number of flax fabric layers had been applied (1, 2, or 3 layers), another parchment paper was placed on the top surface of saturated flax fabric. A scraper was used to remove extra resin and air bubble. Finally, the top face parchment paper was removed, and the correct paper honeycomb core (hollow or foam-filled) was place on the flax fabric. A weighted wooden board also placed on the top of paper honeycomb core to squeeze the extra resin outflow from the sides and make sure the close contact between facing and core. After one day on curing, the

procedure was repeated for the fabrication of the other face. Seven days were needed to make the specimen fully cured before cutting. A band saw was used to cut the sandwich panel into individual specimens with desired size of 1200 mm long and 100 mm wide.

2.4. Test Setup and Instrumentations

Each specimen was tested under a three-point bending setup as shown in Figure 3. The load was applied to the specimen at a rate of 2 mm/min through a 150x150x275 mm Hollow Structure Section (HSS). The HSS was used to distribute the load evenly at the middle of the specimen to avoid the premature local failure. The weight of the HSS was considered during data processing. Two strain gauges were installed at the center of the compression and tension faces to measure the change of longitudinal strain during the test. To ensure that the strain gauge would not be damaged by HSS, a 35 mm diameter hole was cut at the middle of the bottom face of the HSS. A strain potentiometer was applied at the center bottom of the specimen to measure mid-span deflection of the specimens. One support was a roller, and the other one was hinge. A data acquisition system was used to record the applied force, mid-span deflection, and changes of strains on both compression and tension faces at a rate of 10 samples per second. The tests were terminated when either sandwich beam specimens were failed, or the load dropped by 30% from the peak load. The pictures of each failed specimen were taken by camera to identify the failure modes.

3. EXPERIMENTAL RESULTS AND DISCUSSIONS

The main test results are load-deflection, load-strain, and moment-curvature responses of the sandwich beam specimens. Table 2 shows the summary of the test results of each group of the specimens, including: peak load, initial stiffness, initial flexural rigidity, failure modes, and

deflection at peak load. The initial stiffness and initial flexural rigidity were taken as the first linear slope of load-deflection and moment-curvature diagrams, respectively.

3.1. Failure Mode

In this study, two failure modes core shear (CS) and debonding (DB) were observed. Figure 4 shows the examples of each failure mode. The failure mode of each group of the specimens is also noted in Table 2. Most of the specimens failed with core shear. Looking at the specimens with debonding, all of them were specimens with foam-filled honeycomb core. Debonding failure was likely caused by an interfacial crack propagation between the facing and core, which is considered a premature failure. For example, when the specimens 3FL-F-1 and 3FL-F-2 failed by core shear with peak load of 3036 N and 3100 N, the specimen of 3FL-F-3 was failed by debonding with peak load of 997 N. The debonding was likely caused by the weak interfacial bod between the facing and core due to the manual foam-filling method.

3.2. Load-Deflection Behavior

Deflection of beams under applied loads is an important factor to consider in beam design. It could be a governed criterion to meet serviceability limit state requirement. The changes of deflection were captured by a strain potentiometer that was placed at the mid-span of each specimen. The load-deflection behaviors of each specimen are shown in Figure 5. The initial stiffness of each specimen was calculated based the initial slope of load-deflection curve. Because of the non-linear behavior of the specimens, the initial stiffness was calculated by truncating the non-linear tail of the curve until the diagram was close to a line representing the initial stiffness of the specimen. The peak loads and initial stiffness are shown in Table 2 and will be used in the analytical study.

3.3. Moment-Curvature Behavior

Bending moment was calculated at mid-span of each specimen and the curvature was calculated based on the values of strain from two strain gauges applied on the center of each side of the specimens. The curvature φ, was calculated using Eq.1 based on top face strain ε_t, bottom face strain ε_b, and the height of specimen h.

$$\varphi = \frac{\varepsilon_t - \varepsilon_b}{h} \qquad\qquad \text{Eq. 1}$$

3.4. Effect of Honeycomb Core Type

Honeycomb core type is the main parameter in this study. As shown in Figure 6, the change in core type from hollow to foam-filled, peak load and the moment at the peak load increased significantly. For example, looking at the difference between 1FL-F and 1FL-H, 2FL-F and 2FL-H, and 3FL-F and 3FL-H, the peak loads are increased by 51%, 158%, and 210% (ignoring specimen with premature debonding failure). The reason for that is that all the failure modes of specimens were governed by core strength. Therefore, when the core is getting stronger, the load at failure is higher. The honeycomb core type has relatively smaller effect on the initial stiffness and initial flexural rigidity. For example, looking at the difference between 1FL-F and 1FL-H, 2FL-F and 2FL-H, and 3FL-F and 3FL-H, the initial stiffness is increased by 10%, 15%, and 23%, and the initial flexural rigidity almost followed the same pattern. It should be noted that each curve is the average of all identical specimens.

3.5. Effect of Facing Thickness

Facing thickness is another main parameter in this study. The thickness of each layer of flax FRP is around 1.5 mm. As shown in Figure 7, the change of facing thickness had a major impact on the initial stiffness and initial flexural rigidity of each honeycomb core type. For example,

by changing the facing thickness from one to two layers (1FL-F to 2FL-F), the initial stiffness and initial flexural rigidity were increased by 77% and 160%, respectively. However, the failure mode was not changed because the core is always critical, even in the 1-layer specimens. For the specimens with foam-filled core, their peak load and corresponding ultimate moment were increased by adding more flax FRP layers. For example, the peak load and corresponding ultimate moment were increased by 130% and 105%, respectively, from 1FL-F to 2FL-F. On the other hand, for the specimens with hollow core, the increasing of facing thickness did not affect their peak load and ultimate moment. It should be noted that each curve is the average of all identical specimens.

3.6. Comparison of Bio-based and Synthetic Cores

In this section, the mechanical properties of the bio-based core used in this study is compared with those of two different synthetic cores obtained from the literature. As shown in Table 3, the shear modulus and strength of the paper honeycomb (hollow and foam-filled) used in this study are compared with those of two synthetic core materials, namely: recycled polyethylene terephthalate (PET) honeycombs [37] and closed cell polyisocyanurate foams [20]. For a better comparison, the shear modulus and strength values are normalized with the core density of the corresponding core material to obtain specific shear modulus and strength values. The results show that the specific shear strength values are in the same range, however, the specific shear modulus values of the paper honeycomb cores used in this study are higher than those of the synthetic core materials from the literature. For example, the specific shear modulus of the hollow paper honeycomb used in this study is at least two and six times of those of the recycled PET honeycombs and closed cell polyisocyanurate foam.

4. ANALYTICAL STUDY

A new analytical model was developed using the non-linear mechanical properties of each component (facing and core) of the sandwich beams. The model provides the prediction of load-deflection behavior of each sandwich specimen. With the changes of parameters of facing thickness and core types, the model results in different load-deflection curves. The model was used to verify the testing results obtained in the experimental program, and then a parametric was performed on different geometrical parameters.

4.1. Modelling Load-deflection Behavior

The total deflection of a sandwich beam is the sum of the deflection due to bending of facing component and the deflection due to shear of core component. The total deflection equation is shown in Eq. 2.

$$\delta = \delta_b + \delta_s = \frac{PL^3}{48D} + \frac{PL}{4AG} \qquad \text{Eq. 2}$$

In the equation, δ is total mid-span deflection, δ_b is deflection due to bending, δ_s is deflection due to shear. P is the point load applying at the mid-span, L is the span length of beam, D is the flexural stiffness, AG is the shear stiffness of the sandwich beam, G is the shear modulus of the core.

First, a linear model was developed by assuming that elastic modulus of flax FRP and shear modulus of paper honeycomb cores were constant values. The total deflection was calculated by inputting the initial moduli of flax FRP and paper honeycomb cores to Eq. 2. As the stress-strain curves of facing and core components are non-linear, a non-linear model was developed using the secant modulus at any given level of stress as described in the following sections.

4.1.1. Deflection Due to Bending

The stress-strain curve of flax FRP is modeled using the parabolic equation shown in Eq. 3, where σ is stress, ε is strain, E is the initial modulus, σ_u is the ultimate stress, and ε_u is the ultimate strain. All three parameters of E, σ_u, and ε_u were obtained from Betts et al. [20] based on uniaxial tension test results.

$$\sigma = \frac{\sigma_u - E\varepsilon_u}{\varepsilon_u^2}\varepsilon^2 + E\varepsilon \qquad \text{Eq. 3}$$

To develop the non-linear load-deflection curve due to bending, a step-by-step procedure was followed as presented in Figure 8. First, the maximum moment M was calculated at any given load P, and span length of the beam L using Eq. 4 for three-point bending.

$$M = \frac{PL}{4} \qquad \text{Eq. 4}$$

Then, the stress σ resisted by facings was calculated by Eq. 5 based on the beam width b, effective height d (center to center of facings), and facing thickness t.

$$\sigma = \frac{M}{bdt} \qquad \text{Eq. 5}$$

Then, the stress value was plugged into Eq. 3 to obtain the corresponding strain value at each loading step. Once the stress and strain values were obtained, the secant elastic modulus E_{sec} was calculated by Eq. 6.

$$E_{sec} = \frac{\sigma}{\varepsilon} = \frac{\sigma_u - E\varepsilon_u}{\varepsilon_u^2}\varepsilon + E \qquad \text{Eq. 6}$$

The secant elastic modulus was then used to calculate deflection due to bending by Eq. 7. The step-by-step procedure is continued until the peak load is achieved.

$$\delta_b = \frac{PL^3}{48E_{sec}I} \qquad \text{Eq. 7}$$

4.1.2. Deflection Due to Shear

Like the parabolic model of flax FRP, core shear stress-strain curve can also be modeled using a parabolic equation as shown in Eq. 8 to consider its non-linear behavior. In this equation, τ is shear stress, γ is shear strain, G is the initial shear modulus, τ_u is the ultimate shear stress, and γ_u is the ultimate shear strain. All three parameters of G, τ_u, and γ_u were obtained coupon shear tests performed in the experimental section of this study.

$$\tau = \frac{\tau_u - G\gamma_u}{\gamma_u^2}\gamma^2 + G\gamma \qquad \text{Eq. 8}$$

The secant shear modulus G_{sec} was obtained by dividing shear stress by shear strain as follows:

$$G_{sec} = \frac{\tau}{\gamma} = \frac{\tau_u - G\gamma_u}{\gamma_u^2}\gamma + G \qquad \text{Eq. 9}$$

Then, the relation between shear strain and shear deflection δ_s can be found as follows:

$$\tan(\gamma) = \frac{\delta_s}{L/2} = \gamma \qquad \text{Eq. 10}$$

When the value of shear strain, γ, is small, the value of $\tan(\gamma)$ is close to value of γ. Then, plugging Eq. 10 to Eq. 9, the secant shear modulus can be presented as:

$$G_{sec} = \frac{\tau_u - G\gamma_u}{\gamma_u^2}\frac{\delta_s}{L/2} + G \qquad \text{Eq. 11}$$

Then, the shear deflection at each load step was calculated by Eq. 12. The step-by-step procedure is continued until the peak load is achieved. The procedure of modelling the shear deflection is shown in Figure 9.

$$\delta_s = \frac{PL}{4bdG_{sec}} \qquad \text{Eq. 12}$$

4.2. Model Verification

The linear and non-linear numerical models developed in the previous sections were compared to the data obtained in the experimental program. The peak loads at failure in the tests were used as the end point of model in this section. The verification diagrams are shown in Figure 10. As shown in the figure, both linear and non-linear model are accurate at the initial part of

load-deflection curve. However, by increasing the load, the load-deflection relations of the specimens become more non-linear, and the linear model gradually becomes less accurate than non-linear model.

4.3. Failure Prediction

The failure mode and peak load at failure of each specimen are predicted in this section. Overall, three main failure modes facing tensile rupture (TR), core shear (CS), and compression face wrinkling (WR) are considered. By plugging in the parameters of specimen dimension and material properties from facing and core components tests, the peak load at failure of each failure criteria can be calculated using Eqs. 13-15 from literature [38][39]. In the equations, E_c is the core modulus, G_c is the core shear modulus, and E_f is the facing modulus. The other parameters have already been defined in previous sections. The failure criteria with minimum peak load at failure is considered as critical failure modes. Using the equations, the predicted peak loads and the critical failure modes of the specimen tested in the experimental program and compared to the experimental results as shown in Table 4. It should be highlighted that the peak load equations have been set for conventional sandwich composites with linear-elastic behavior. As the bio-based sandwich composites exhibit nonlinear behavior, the failure prediction based on the conventional equations is not accurate. Thus, in the future, a new set of peak load equations should be developed to account for the material non-linearity.

$$P_{FR} = \frac{4\sigma_u bct}{L} \qquad \text{Eq. 13}$$

$$P_{CS} = \frac{2\tau_u bc}{\sqrt{(\frac{LE_c}{4tE_f})^2 + 1}} \qquad \text{Eq. 14}$$

$$P_{WR} = \frac{2tdb}{L} \sqrt[3]{E_f E_c G_c} \qquad\qquad \text{Eq. 15}$$

4.4. Parametric Study

A parametric study was conducted on sandwich beams made from flax FRP facings and paper honeycomb cores. Only six groups of these sandwich beams were tested in the experimental program. Thus, to consider other cases, four parameters were considered in parametric study: core thickness c, facing thickness t, unsupported span length L, and type of core (hollow and foam-filled). The parameters are presented into three groups: i) t = 3 mm, L = 1 m, and changing variable c (75, 100, 125, and 150 mm); ii) c = 150 mm, L = 1 m, and changing variable t (3, 6, 9, and 12 mm); and iii) t = 3 mm, c = 150 mm, and changing variable L (1 , 2 , 3 , and 4 m).

4.4.1. Effect of Core Thickness

The range of core thicknesses studied was 75 to 150 mm, while the facing thickness t and unsupported span length L were constant (t = 3 mm, L = 1 m) for both hollow and foam-filled cores. Figure 11 shows the variation of load vs deflection at mid-span and load vs. tensile and compressive strains at mid-span. The figure indicates that the load capacity and stiffness of the beams increased as the core thickness increased. The peak load of all the beams were governed by the core shear capacity. Also, comparing to the sandwich beam with hollow core, the sandwich beams with foam-filled core show a higher load capacity, higher stiffness, and higher total deflection and facing strain at failure. In addition, the nonlinear behavior become more dominant as the core thickness increased. Overall, by doubling the core thickness, the loading capacity of the beams were almost doubled, regardless of foam-filling. In addition, the beams with foam-filled cores had always a loading capacity approximately 60% higher that that of the beams with hollow cores.

4.4.2. Effect of Facing Thickness

The range of facing thicknesses studied was 3 to 12 mm, while the core thickness and unsupported span length were constant (c = 150 mm, L = 1 m) for both hollow and foam-filled cores as shown in Figure 12. It shows that by adding thicker facing component, the stiffness of the sandwich beam was increased. However, the load capacities of the beams were not improved because the core shear governed the failure. Also, as the facing thickness increased, the non-linearity of the curves decreased, especially for foam-filled core sandwich beams. The reason of that is that the facing strains at failure decreased with the thicker facing applied, so the stress-strain behavior of the facing component was infinitely close to a straight line with a slope of its initial modulus.

4.4.3. Effect of Span Length

The range of unsupported span lengths analysed was at a range between 1 to 4 m, while core thickness and facing thickness were (constant t = 3 mm, c = 150 mm). The behavior of the sandwich beams with respect to varying facing thickness and core type are shown in Figure 13. It indicates that the load capacities and stiffness of the beams were sharply decreased by increasing the span length. On the other hand, the deflections the beams were obviously increased at failure. Also, the failure mode turned to tension facing rupture from core shear when unsupported span length increased.

5. FUTURE STUDIES

This study was focused on medium-scale bio-based sandwich beams under quasi-static loading based on available core materials at the time of the research. It is suggested to test the full-scale of the sandwich beams (using different core thicknesses and beam geometries) and verify the

proposed analytical model against the full-scale test results. Also, testing of the bio-based sandwich beams under impact and fatigue loading is suggested. In addition, as the bond between the FRP facing and the core materials is significantly influenced by the surface texture of the core, it is suggested to study the effect of a factory-based foam-filling method of the honeycomb cores rather than the manual foam-filling method used in this study. This study also showed that the bio-based sandwich composites exhibit non-linear behavior as opposed to conventional sandwich composites made of synthetic material. As a result, new specifications and simplified design equations are needed to account for the material non-linearity.

6. CONCLUSIONS

In this study, a total of 18 sandwich beams were fabricated by bio-based materials, tested under three-point bending, and modeled via an analytical study. The main contribution of this study to the field is taking bio-based sandwich composites to the next level by sandwiching a paper honeycomb core between facings made of a flax fabric and bio-based epoxy resin. Two types of paper honeycomb cores of hollow and foam-filled were used to evaluate the effect of foam filling on strength and stiffness of the sandwich beams. Also, an analytical model was developed to predict the non-linear behavior of the bio-based sandwich beams. The following conclusions cab be drawn:

- Both flax FRP facing and paper honeycomb core showed non-linear behavior, which should be considered in analysis and design.

- Foam-filling was effective in increasing the shear modulus and strength of the paper honeycomb 24 and 60% respectively.

- Foam-filling showed limited effect on the initial stiffness of the sandwich beams due to the

dominant role of facings, but it increased the peak loads of 1-, 2-, and 3-layer sandwich beams by 51, 158, and 210%, respectively, with respect to corresponding the beams made of hollow paper honeycomb core.

- The parameter of facing thickness had major impact on the initial stiffness and initial flexural rigidity, increasing them by 77 and 160%, respectively, by changing the facing thickness from 1 to 2 layers of flax fabric.

- Almost all the sandwich beams were failed by core shear failure mode, and two sandwich beams with foam-filled core were failed by premature debonding failure. The debonding failure was caused by pre-existing crack between core and facing component. The pre-existing crack was likely due to manual method of filling the hollow honeycomb core with spray foam.

- According to parametric study on the sandwich beams, increasing the core thickness from 75 to 150 mm doubled the loading capacity of the beams with paper honeycomb cores, regardless of foam-filling, however the beams with foam-filled cores had always a loading capacity approximately 60% higher than that of the beams with hollow cores. Span length is an important parameter that can switch the failure mode from core shear to facing tensile rupture.

- Although the bio-based sandwich system showed potential for building applications, future research is suggested on factory-based foam-filling method of the paper honeycomb cores and testing full-scale sandwich beams using different core thicknesses and beam geometries for further verification of the proposed non-linear model. Also, testing of the bio-based sandwich system under impact and fatigue loading is suggested. Moreover, peak load

equations of sandwich composites should be updated based on the non-linear behavior of bio-based materials.

7. REFERENCES

[1]   Statista. (2018). 13,000 Buildings Per day. Learn why the construction industry needs to build an average of 13,000 buildings every day through 2050.

[2]   Yadav, M., & Agarwal, M. (2021). Biobased building materials for sustainable future: An overview. Materials Today : Proceedings, 43, 2895-2902.

[3]   Babu, R., O'Connor, K., & Seeram, R. (2013). Current progress on bio-based polymers and their future trends. Progress in Biomaterials, 2(1), 1-16.

[4]   Baraghith, A. T., Mansour, W., Behiry, R. N., & Fayed, S. (2022). Effectiveness of SHCC strips reinforced with glass fiber textile mesh layers for shear strengthening of RC beams: Experimental and numerical assessments. Construction and Building Materials, 327, 127036.

[5]   Fayed, S., & Mansour, W. (2020). Evaluate the effect of steel, polypropylene and recycled plastic fibers on concrete properties. Advances in concrete construction, 10(4), 319-332.

[6]   Mansour, W., & Fayed, S. (2021). Flexural rigidity and ductility of RC beams reinforced with steel and recycled plastic fibers. Steel and Composite Structures, 41(3), 317-334.

[7]   Li, Y., Li, C., He, J., Gao, Y., & Hu, Z. (2020). Effect of functionalized nano-SiO2 addition on bond behavior of adhesively bonded CFRP-steel double-lap joint. Construction and Building Materials, 244, 118400.

[8]   Cywar, R. M., Rorrer, N. A., Hoyt, C. B., Beckham, G. T., & Chen, E. Y. X. (2022). Bio-

based polymers with performance-advantaged properties. Nature Reviews Materials, 7(2), 83-103.

[9]   Sparnins. E. (2009). Mechanical properties of flax fibers and their composites. University of Technology, Department of Engineering Sciences and Mathematics, Material Science.

[10]   Faruk, O., Bledzki, A., Fink, H., & Sain, M. (2012). Biocomposites reinforced with natural fibers: 2000–2010. Progress in Polymer Science, 37(11), 1552-1596.

[11]   Rajesh, M., Pitchaimani, J., & Rajini, N. (2016). Free Vibration Characteristics of Banana/Sisal Natural Fibers Reinforced Hybrid Polymer Composite Beam. Procedia Engineering, 144, 1055-1059.

[12]   Becker, J., & Wittmann, C. (2015). Advanced biotechnology: Metabolically engineered cells for the bio-based production of chemicals and fuels, materials, and health-care products. Angewandte Chemie International Edition, 54(11), 3328-3350.

[13]   Omonov, T., & Curtis, J. (2014). Biobased epoxy resin from canola oil. Journal of Applied Polymer Science, 131(8), N/a.

[14]   Adekunle, K., Cho, S., Ketzscher, R., & Skrifvars, M. (2012). Mechanical properties of natural fiber hybrid composites based on renewable thermoset resins derived from soybean oil, for use in technical applications. Journal of Applied Polymer Science, 124(6), 4530-4541.

[15]   Hosseini, N., Webster, D., & Ulven, C. (2016). Advanced biocomposite from highly functional methacrylated epoxidized sucrose soyate (MAESS) resin derived from vegetable oil and fiberglass fabric for composite applications. European Polymer Journal, 79, 63-71.

[16] Sadeghian, P., Hristozov, D., & Wroblewski, L. (2018). Experimental and analytical behavior of sandwich composite beams: Comparison of natural and synthetic materials. The Journal of Sandwich Structures & Materials, 20(3), 287-307.

[17] ISIS Canada. (2006). An introduction to FRP Composites for Construction. ISIS Educational Module 2. Structural Innovation and Monitoring Technologies Resource Centre.

[18] Florence, A., Jaswin, M., Arul Prakash, M., & Jayaram, R. (2020). Effect of energy-absorbing materials on the mechanical behaviour of hybrid FRP honeycomb core sandwich composites. Materials Research Innovations, 24(4), 244-255.

[19] MacDonnell, L., & Sadeghian, P. (2020). Experimental and analytical behaviour of sandwich composites with glass fiber-reinforced polymer facings and layered fiber mat cores. Journal of Composite Materials, 54(30), 4875-4887.

[20] Betts, D., Sadeghian, P., & Fam, A. (2018). Experimental Behavior and Design-Oriented Analysis of Sandwich Beams with Bio-Based Composite Facings and Foam Cores. Journal of Composites for Construction, 22(4), 4018020.

[21] Ramesh, M., Palanikumar, K., & Reddy, K. (2017). Plant fibre based bio-composites: Sustainable and renewable green materials. Renewable & Sustainable Energy Reviews, 79, 558-584.

[22] Wang, Z. (2019). Recent advances in novel metallic honeycomb structure. Composites. Part B, Engineering, 166, 731-741.

[23] Asprone, D., Auricchio, F., Menna, C., Morganti, S., Prota, A., & Reali, A. (2013). Statistical finite element analysis of the buckling behavior of honeycomb structures.

Composite Structures, 105, 240-255.

[24] McCracken, A., & Sadeghian, P. (2018). Corrugated cardboard core sandwich beams with bio-based flax fiber composite skins. Journal of Building Engineering, 20, 114-122.

[25] Fam, A., Sharaf, T., & Sadeghian, P. (2016). Fiber element model of sandwich panels with soft cores and composite skins in bending considering large shear deformations and localized skin wrinkling. Journal of Engineering Mechanics, 142(5), 04016015.

[26] Mathieson, H., & Fam, A. (2014). High cycle fatigue under reversed bending of sandwich panels with GFRP skins and polyurethane foam core. Composite Structures, 113, 31-39.

[27] Manalo, A. C. (2013). Behaviour of fibre composite sandwich structures under short and asymmetrical beam shear tests. Composite structures, 99, 339-349.

[28] Ferdous, W., Manalo, A., Aravinthan, T., & Fam, A. (2018). Flexural and shear behaviour of layered sandwich beams. Construction and Building Materials, 173, 429-442.

[29] Betts, D., Sadeghian, P., & Fam, A. (2021). Experiments and nonlinear analysis of the impact behaviour of sandwich panels constructed with flax fibre-reinforced polymer faces and foam cores. Journal of Sandwich Structures & Materials, 23(7), 3139-3163.

[30] Betts, D., Sadeghian, P., & Fam, A. (2021). Post-impact residual strength and resilience of sandwich panels with natural fiber composite faces. Journal of Building Engineering, 38, 102184.

[31] CoDyre, L., Mak, K., & Fam, A. (2018). Flexural and axial behaviour of sandwich panels with bio-based flax fibre-reinforced polymer skins and various foam core densities. Journal of Sandwich Structures & Materials, 20(5), 595-616.

[32] Betts, D., Sadeghian, P., & Fam, A. (2020). Structural behavior of sandwich beams

withflax fiber–reinforced polymer faces and cardboard cores under monotonic and impact loads. Journal of Architectural Engineering.

[33] Monti, A., El Mahi, A., Jendli, Z., & Guillaumat, L. (2017). Experimental and finite elements analysis of the vibration behaviour of a bio-based composite sandwich beam. Composites Part B: Engineering, 110, 466-475.

[34] Fu, Y., & Sadeghian, P. (2020). Flexural and shear characteristics of bio-based sandwich beams made of hollow and foam-filled paper honeycomb cores and flax fiber composite skins. Thin-walled Structures, 153, 106834.

[35] ASTM D3039 (2014). Standard test method for tensile properties of polymer matrix composite materials. American Society for Testing and Materials, West Conshohocken, PA, USA.

[36] ASTM D273 (2020). Standard test method for shear properties of sandwich core materials. American Society for Testing and Materials, West Conshohocken, PA, USA.

[37] Kassab, R. & Sadeghian, P. (2023). Effects of Material Non-linearity on the Structural Performance of Sandwich Beams made of Recycled PET Foam Core and PET Fiber Composite Facings: Experimental and Analytical Studies. Structures, under review.

[38] Triantafillou, T. C., and Gibson, L. J. (1987). "Failure Mode Maps for Foam-Core Sandwich Beams." Materials Science and Engineering, 95, 37–53.

[39] Yusuff, S. (1955). Theory of wrinkling in sandwich construction. The Aeronautical Journal, 59(529), 30-36.

Table 1. Test matrix.

Group No.	Specimen ID	Number of FFRP layers in each facing	Core type	Number of Specimens
1	1FL-H	1	Hollow	3
2	1FL-F	1	Foam Filled	3
3	2FL-H	2	Hollow	3
4	2FL-F	2	Foam Filled	3
5	3FL-H	3	Hollow	3
6	3FL-F	3	Foam Filled	3
Total				18

Note: H =Hollow; F = Foam-filled

Table 2. Summary of test results.

Specimen Group ID	Peak load (N)		Stiffness (kN/m)		Flexural Rigidity (kN-m^2)		Failure Modes	Deflection at Peak load (mm)	
	AVG	COV (%)	AVG	COV (%)	AVG	COV (%)		AVG	COV (%)
1FL-F	1040	39.8	94.8	4.7	2.5	16.0	CS/DB	12.45	36.9
1FL-H	898	19.8	86.3	6.6	2.6	6.7	CS	12.76	21.6
2FL-F	2392	19.7	167.8	4.5	6.5	10.3	CS/DB	16.74	6.5
2FL-H	926	26.6	146.1	6.9	5.5	5.8	CS	11.55	30.3
3FL-F	2378	50.3	216.2	4.7	8.4	21.9	CS/DB	12.65	48.0
3FL-H	990	14.6	176.1	6.8	5.7	6.3	CS	7.33	10.2

Note: The average peak loads ignoring the specimens with debonding failure for 1FL-F and 3FL-F are 1358 N and 3068 N, respectively. CS = Core shear; DB = Debonding.

Table 3. Comparison of paper honeycomb used in this study and synthetic cores from the literature.

Core type	Reference	Density (kg/m^3)	Shear modulus (MPa)	Specific shear modulus *	Shear Strength (KPa)	Specific shear strength **
Honeycomb, paper, hollow	Current study	19	10.24	0.54	150	7.89
Honeycomb, paper, foam-filled	Current study	44	12.73	0.29	240	5.45
Honeycomb, recycled PET, hollow	[37]	70	12.70	0.18	500	7.14
Honeycomb, recycled PET, hollow	[37]	80	20.80	0.26	600	7.50
Foam, closed cell polyisocyanurate	[20]	32	2.07	0.06	170	5.31
Foam, closed cell polyisocyanurate	[20]	64	5.86	0.09	580	9.06

* Unit: MPa/kg/m^3

** Unit: KPa/kg/m^3

Table 4. Comparison of data obtained from test and model.

Case #	Specimen Group ID	Peak load (N)				Failure Modes		Deflection at Peak load			
		Test		Model	T/M	Test	Model	Test		Model	T/M
		AVG	SD					AVG	SD		
1	1FL-F	1040	413	1975	0.53	CS/DB	TR	12.4	4.6	26.8	0.46
2	1FL-H	898	178	1975	0.45	CS	TR	12.8	2.8	30.4	0.42
3	2FL-F	2392	472	3692	0.65	CS/DB	CS	16.7	1.1	28.7	0.58
4	2FL-H	926	246	2306	0.40	CS	CS	11.6	3.5	21.3	0.54
5	3FL-F	2377	1196	3692	0.64	CS/DB	CS	12.6	6.1	20.5	0.62
6	3FL-H	990	144	2306	0.43	CS	CS	7.3	0.8	17.0	0.43

T/M= Test to Model Ratio; CS=Core Shear; DB=Debonding; TR=Tension Rupture
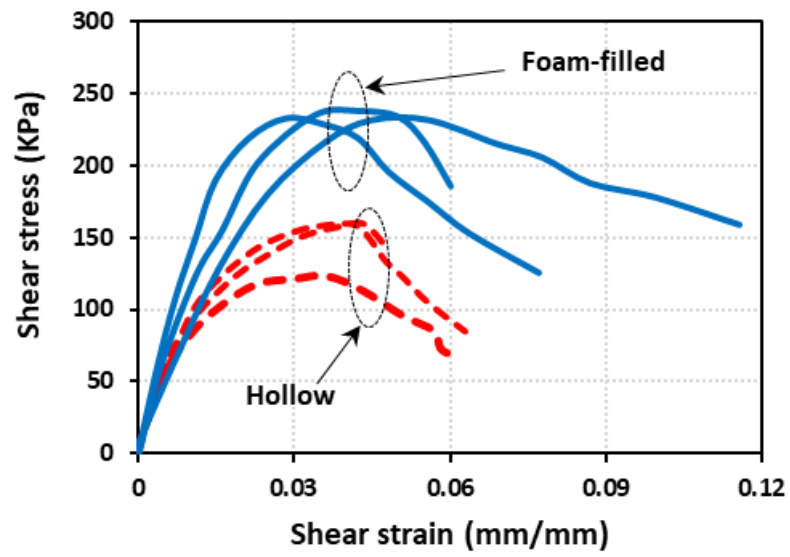
Figure 1. Stress-strain behavior of paper honeycomb cores in shear.
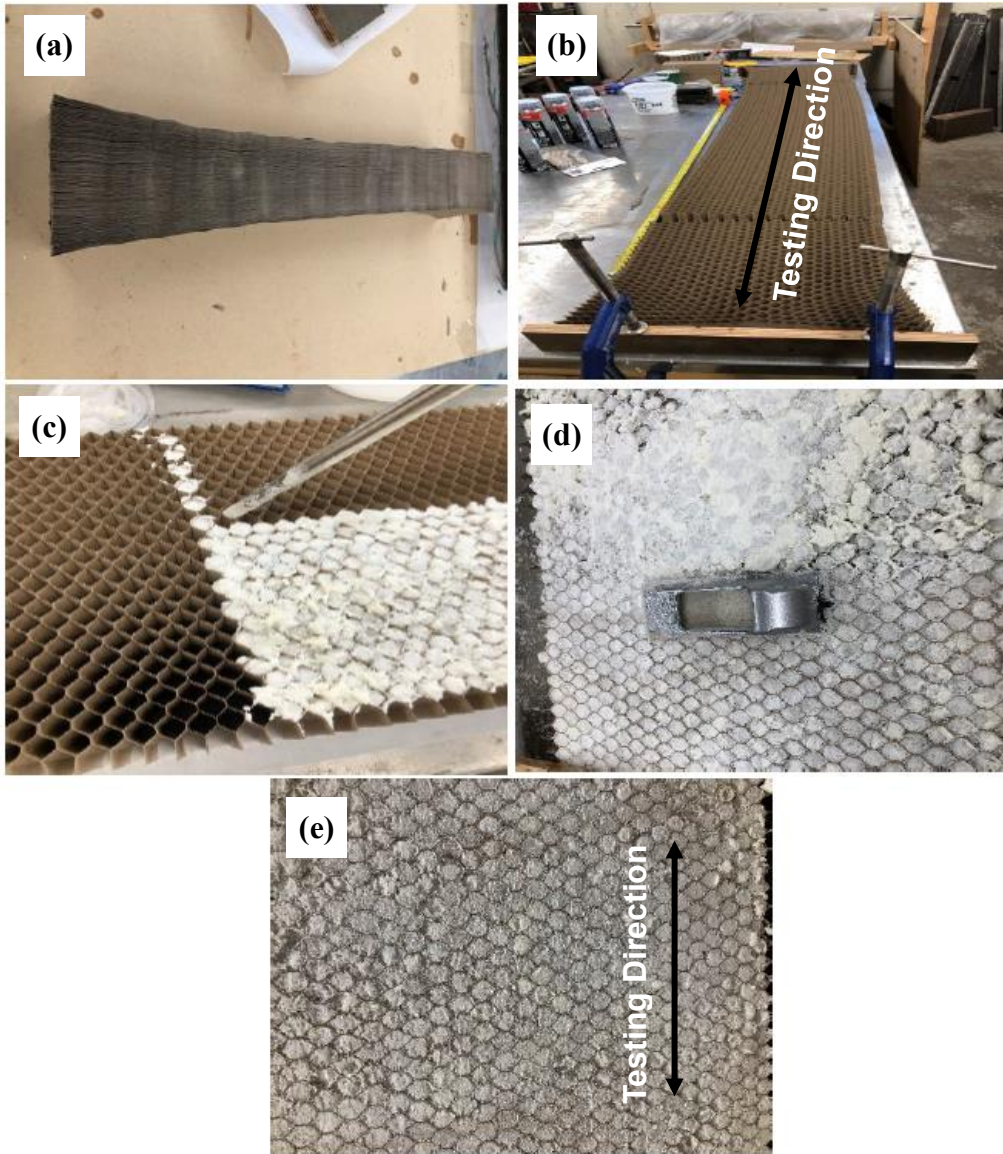
Figure 2. Foam filling: a) unstretched paper honeycomb core; b) stretched paper honeycomb core; c) filling foam with dispensing gun; d) removal extra foam; e) finished foam-filled core.
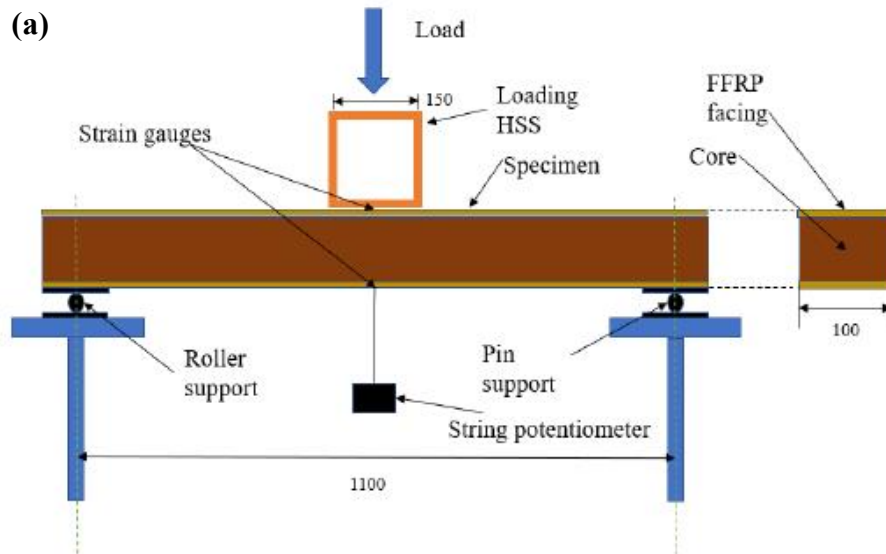
Figure 3. Test setup and instrumentation: a) schematic drawing (dimensions in mm); b) test setup photo.
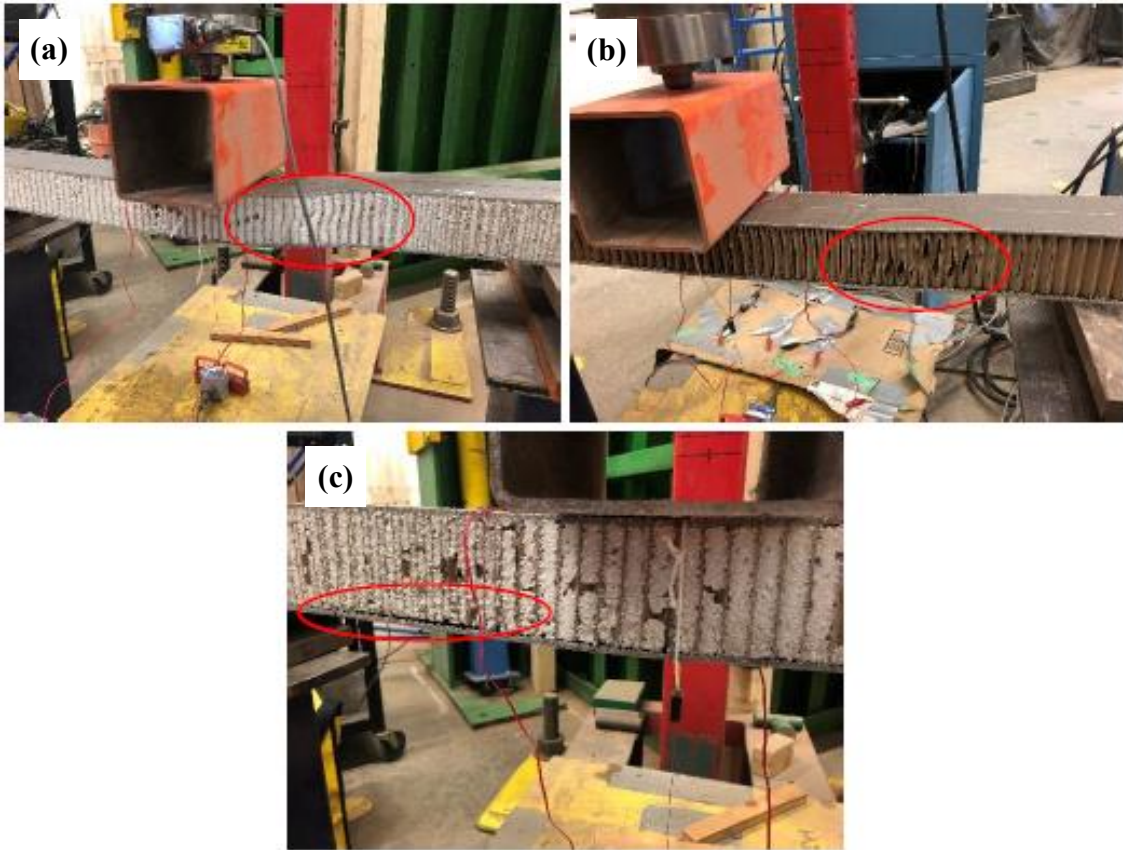
Figure 4. Examples of failure modes: a) core shear failure of foam-filled core; b) core shear failure of hollow core; c) debonding failure of foam-filled core.
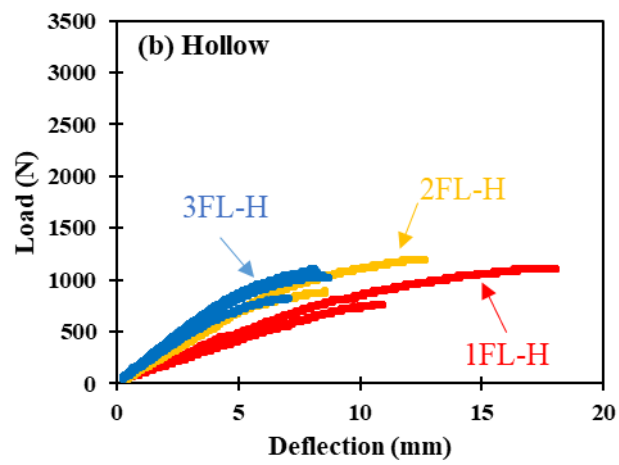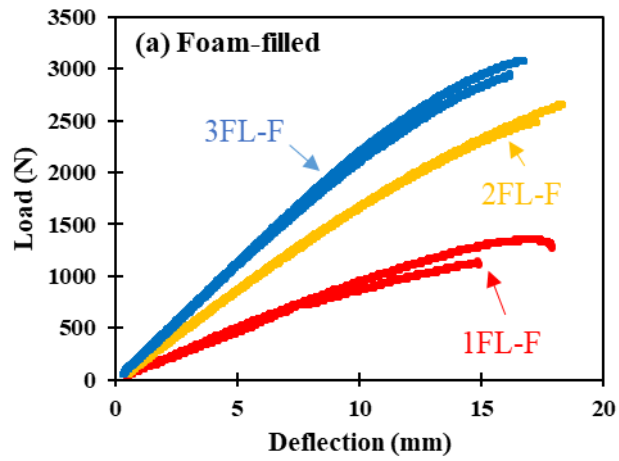
Figure 5. Load-deflection behavior of specimens with (a) foam-filled and (b) hollow paper honeycomb core.
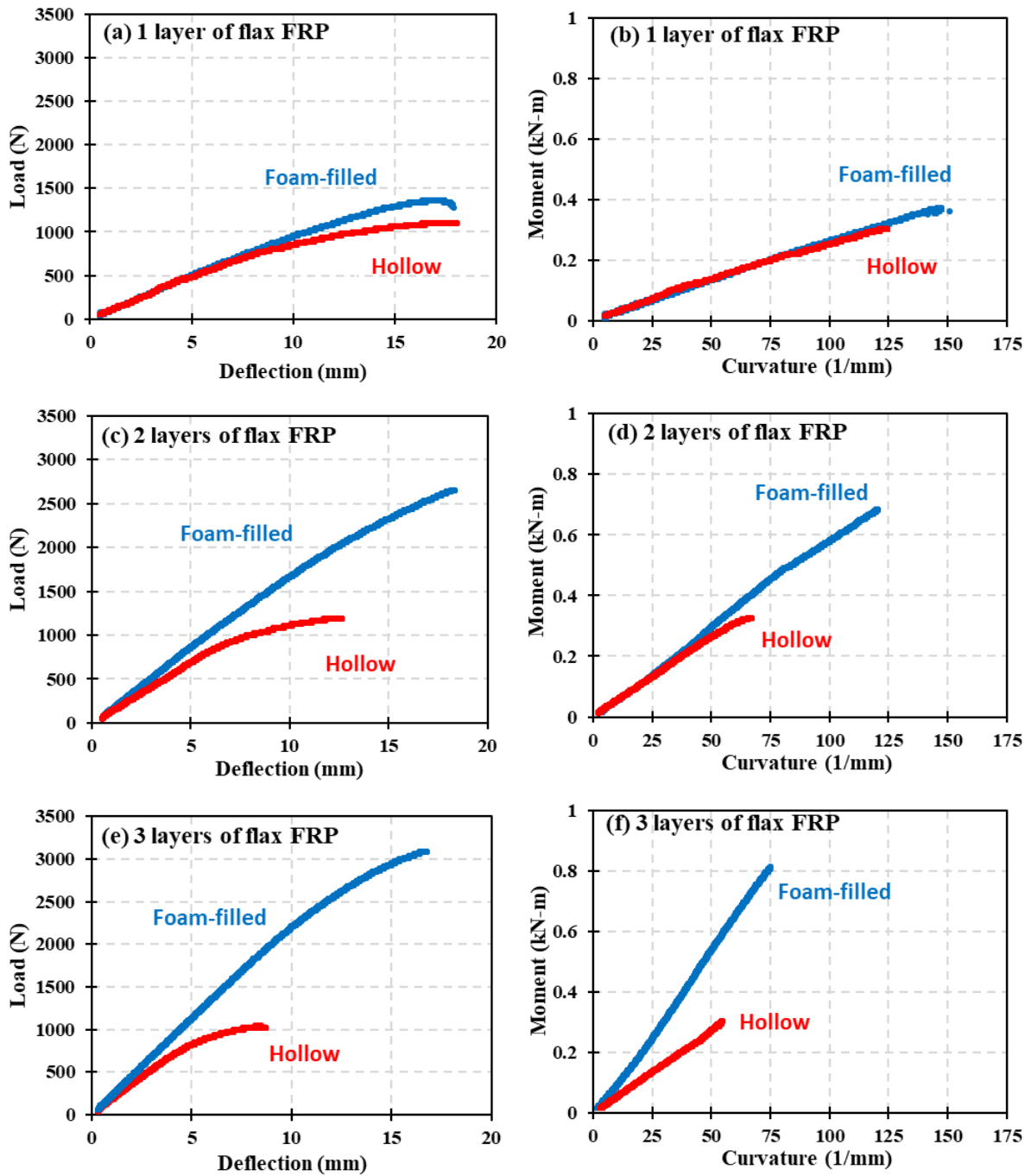
Figure 6. Effect of honeycomb core type on load-deflection and moment-curvature diagrams: (a-b) 1 layer of flax FRP; (c-d) 2 layers of flax FRP; and (e-f) and 2 layers of flax FRP.
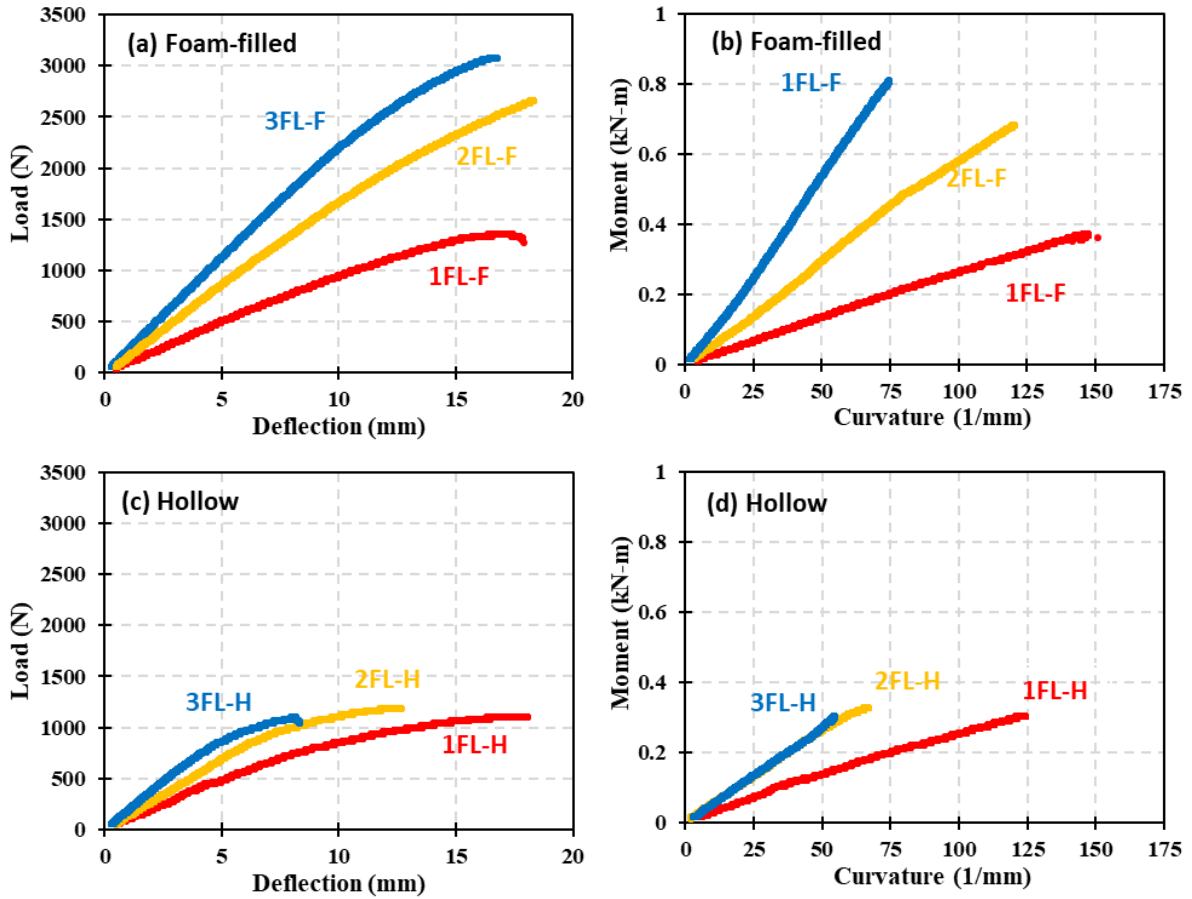
Figure 7: Effect of facing thickness on load-deflection and moment-curvature diagrams: (a-b) foam-filled core; and (c-d) hollow core.
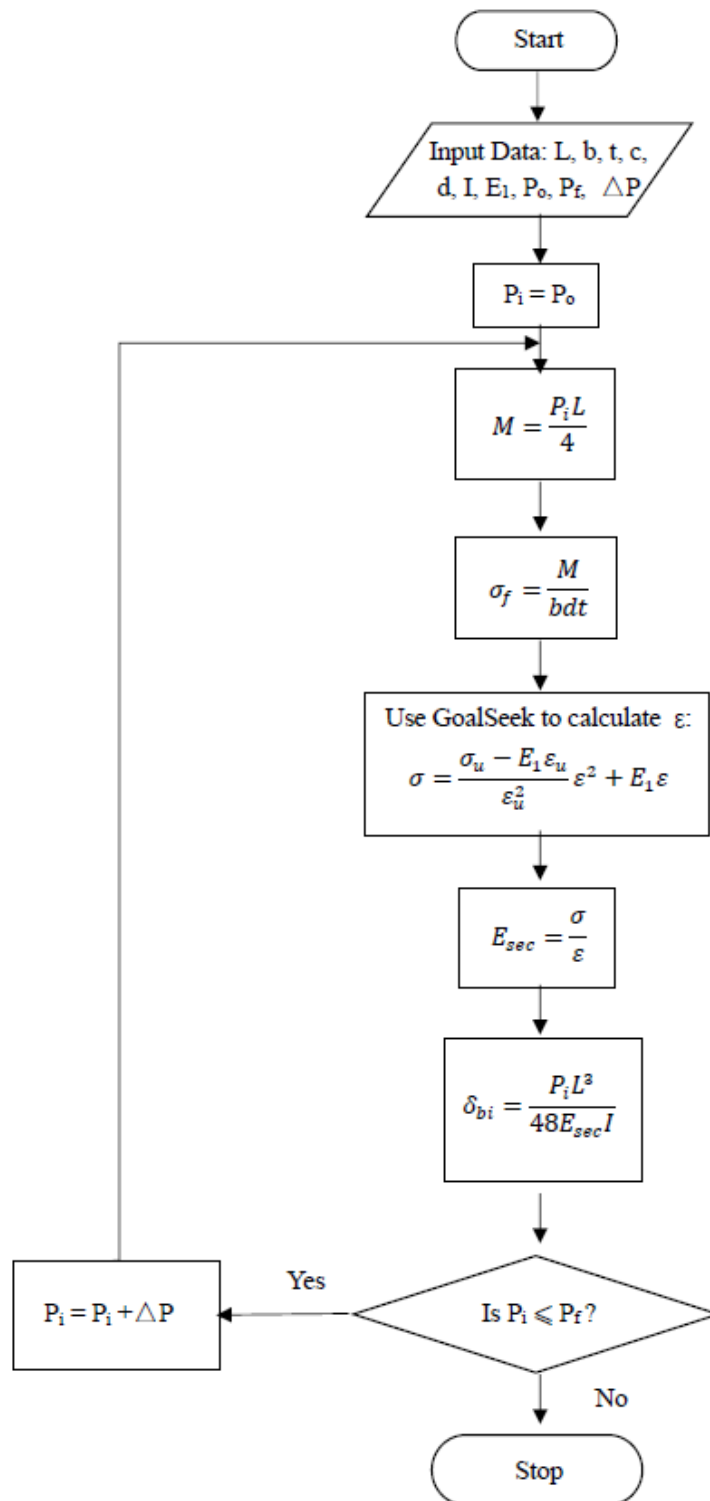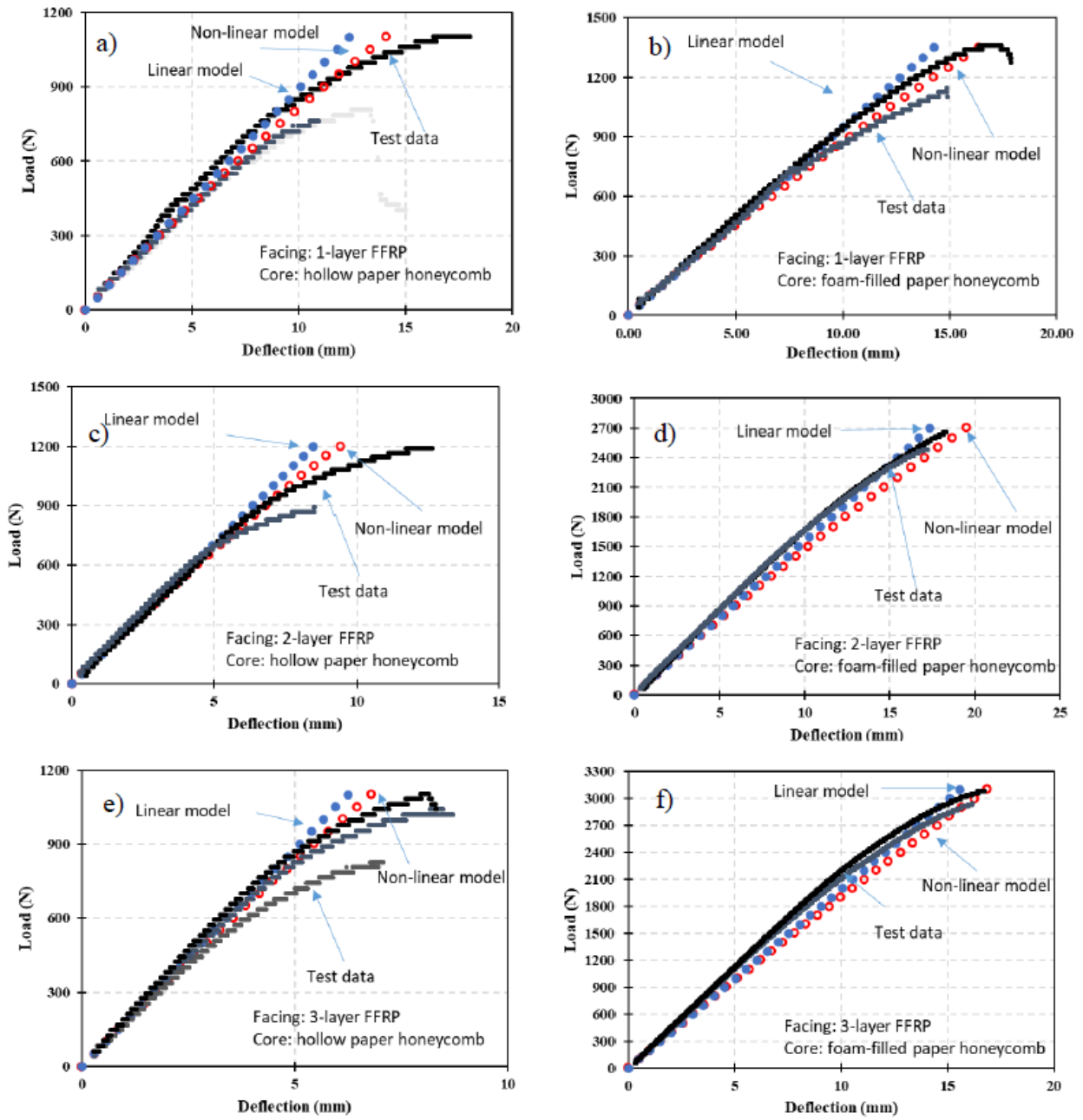
Figure 8. Flowchart of deflection model due to bending.
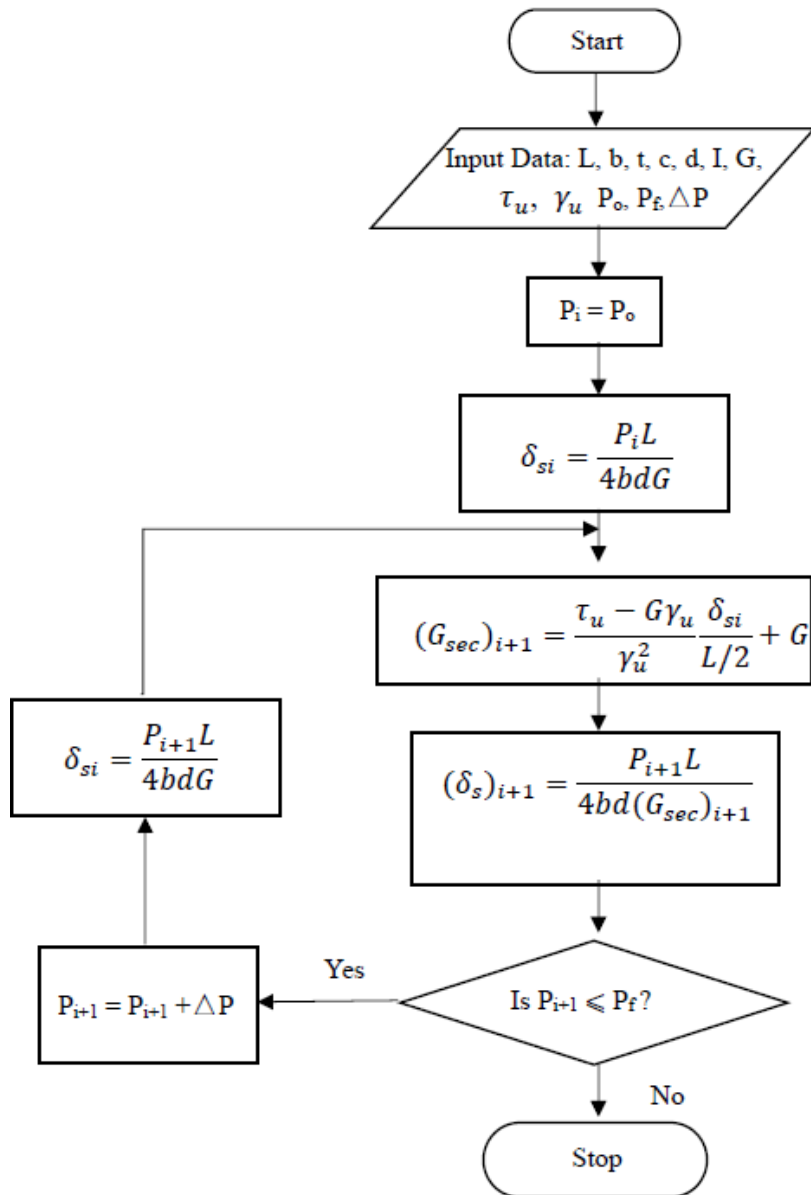
Figure 9. Flowchart of deflection model due to shear.

Figure 10. Load-deflection curve comparison between linear model, non-linear model, and test data: a) 1FL-H; b) 1FL-F; c) 2FL-H; d) 2FL-F; e) 3FL-H; f) 3FL-F.
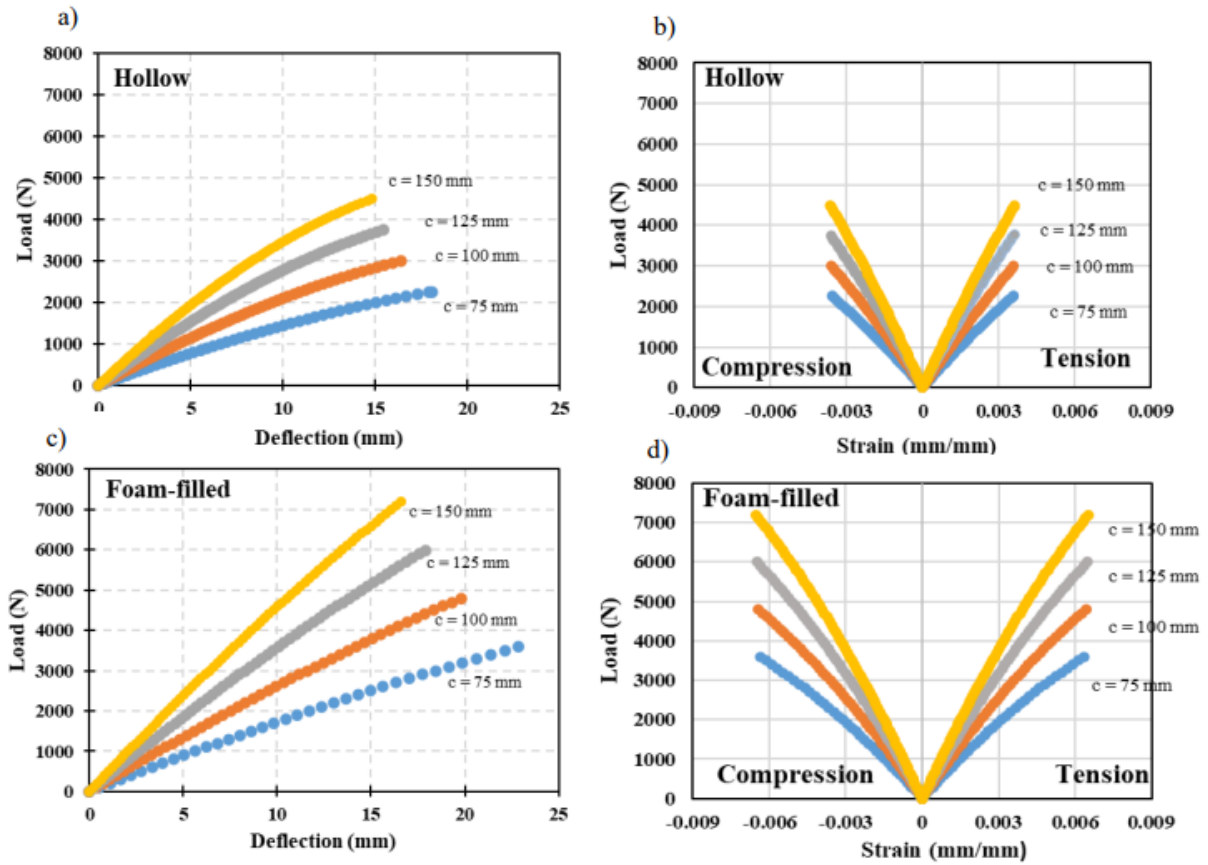
Figure 11. Parametric study with varying core thickness and core type: (a-b) hollow paper honeycomb core; and (c-d) foam-filled paper honeycomb core (constant parameters: t = 3 mm, L = 1 m).
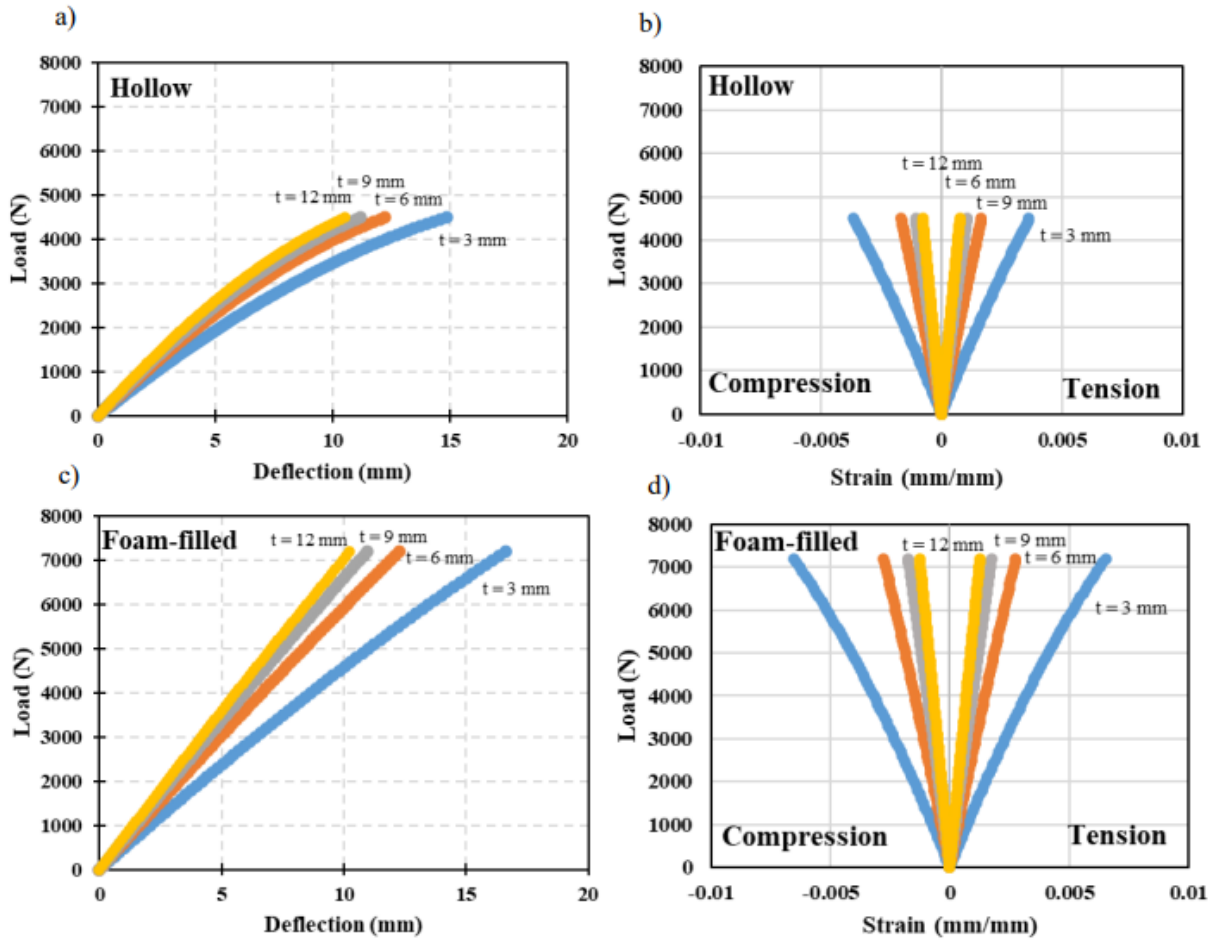
Figure 12. Parametric study with varying facing thickness and core type: (a-b) hollow paper honeycomb core; and (c-d) foam-filled paper honeycomb core (constant parameters: c = 150 mm, L = 1 m).
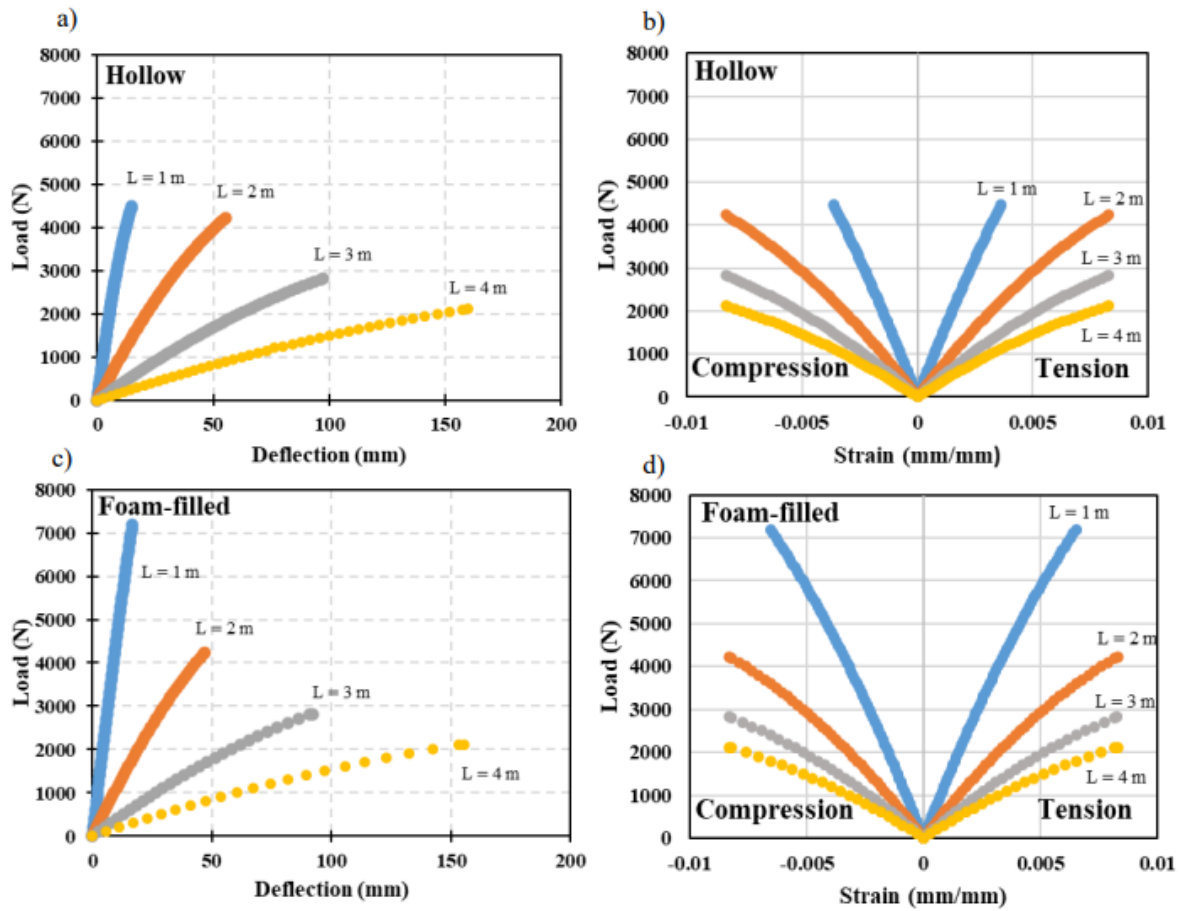
Figure 13. Parametric study with varying unsupported span length and core type: (a-b) hollow paper honeycomb core; and (c-d) foam-filled paper honeycomb core (constant parameters: t = 3 mm, c = 150 mm)